ACS Photonics

pubs.acs.org/journal/apchd5

Letter

Nanoscale Infrared Spectroscopy and Imaging of Catalytic Reactions in Cu_2O Crystals

G. X. Ni, S. Chen, S. S. Sunku, A. Sternbach, A. S. McLeod, L. Xiong, M. M. Fogler, G. Chen,* and D. N. Basov*

Cite This: *ACS Photonics* 2020, 7, 576–580

Read Online

ACCESS | Metrics & More | Article Recommendations | Supporting Information

ABSTRACT: Many of the existing electrochemical catalysts suffer from poor selectivity, instability, and low exchange current densities. These shortcomings call for a comprehensive exploration of the catalytic processes at the fundamental nanometer length scale levels. Here we exploit infrared (IR) nanoimaging and nanospectroscopy to directly visualize catalytic reactions on the surface of Cu_2O polyhedral single crystals with nanoscale spatial resolution. Nano-IR data revealed signatures of this common catalyst after electrochemical reduction of carbon dioxides (CO_2). We discuss the utility of nano-IR methods for surface/facet engineering of efficient electrochemical catalysts.

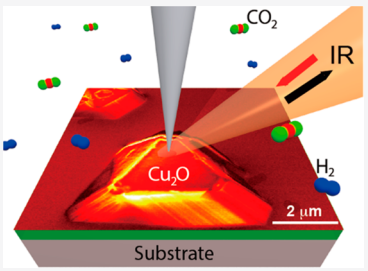

KEYWORDS: *CO_2 reduction, Cu_2O catalysis, scanning nano-optical imaging, infrared nanospectroscopy, s-SNOM*

Progress with improving electrocatalytic conversion efficiency requires careful examination of factors impacting the reactivity, selectivity, and lifetime of catalysts down to the nanoscale.[1−10] A few advanced approaches have been developed to investigate these factors including in situ microscopy and electrochemical techniques.[11−13] However, these methods are commonly complicated and destructive to the catalyst itself. Conventional optical characterization tools, i.e., IR, visible, and Raman spectroscopy, can provide critical insight into the catalytic reactions without disrupting catalytic processes, but their spatial resolution is limited to the 1−10 μm scales. Here we investigated nanocrystallites of cuprous oxide (Cu_2O) catalysts using nano-optical means. This nascent experimental method enables a direct visualization of both specimens' morphologies and catalytic reactions on the surface of particles within 25 nm spatial resolution.[14,15]

Electrochemical reduction of CO_2 into valuable fuels and chemicals has potential to be scaled up.[16,17] Cheap and earth-abundant Cu_2O had been shown to be an excellent CO_2 reduction catalyst in aqueous media by electrochemical, photochemical, and photo-electrochemical methods.[18,19] Earlier studies revealed that the coexistence of Cu_2O on the Cu surface preferentially produced hydrocarbons during electrochemical reduction of CO_2.[20] Recent studies demonstrated that the mixed surface oxidation state of Cu_2O nanocubes might facilitate CO_2 reduction in the gas phase via heterogeneous photocatalytic hydrogenation.[21] However, to date, it is still unclear how the catalytic reaction happens in a Cu_2O catalyst at the nanoscale. For the first time, we employed Cu_2O polyhedral microcrystals to act as catalysts for electrochemical reduction of CO_2. In our experiments, we systematically monitored Cu_2O polyhedral microcrystals before and after chemical reactions using both nano-IR imaging and nano-IR spectroscopy methods. Our experimental results, augmented with theoretical modeling, have uncovered the factors governing catalysis dynamics of Cu_2O polyhedral microcatalysts and also validated IR nanoscopy as a unique probe of catalysis.

We utilized scanning near-field nano-IR microscopy to investigate the critical catalysis processes. This unique nano-IR technique has been routinely utilized for detecting surface polaritons in two-dimensional materials as well as for visualizing inhomogeneities in complex oxides[22,23] along with many other applications in chemistry and biology.[24,25] Figure 1a shows a schematic of our nano-optical setup where IR light of frequency ω is focused onto the apex of a metallized tip. The tip functions as an optical antenna that intensifies the incident electric field at its apex and generates an evanescent field beneath the tip, which penetrates tens of nanometers into the Cu_2O samples.[26,27] The spatial resolution of a nanoimaging apparatus is determined by the radius of curvature at the tip apex (<25 nm) and is independent of the IR wavelength. In our nano-IR studies, both pseudoheterodyne detection at the third harmonics (nanoimaging) and an asymmetric Michelson interferometer for Fourier transform infrared spectroscopy (nano-FTIR) are interchangeable. The amplitude of the backscattered signal $s(\omega)$ and its phase $\phi(\omega)$ are recorded using an interferometric detection,[28,29] allowing the extraction

Received: December 3, 2019
Published: February 14, 2020

https://dx.doi.org/10.1021/acsphotonics.9b01704
ACS Photonics 2020, 7, 576–580

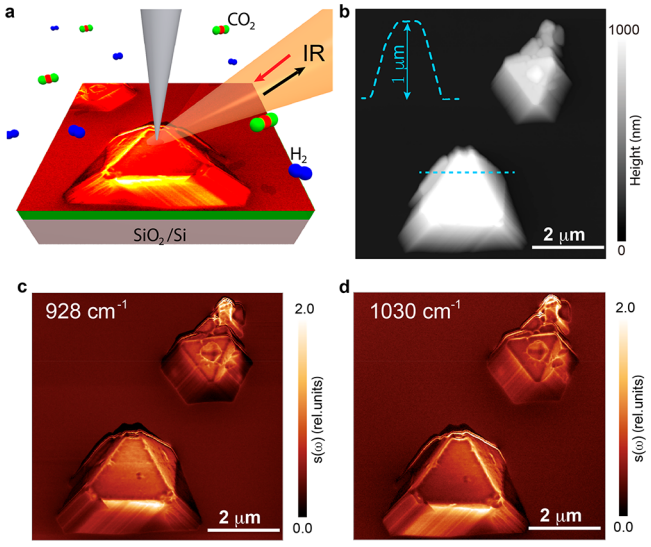

Figure 1. Topographic and nano-IR imaging of Cu_2O microcrystals. (a) Schematic of the IR nanoimaging experiment, showing the metallic nanoprobe tip illuminated by an IR laser beam. Cu_2O microcrystals were exposed to CO_2 (white and red) and released H_2(blue). (b) Atomic force microscope topography image of Cu_2O crystals. Inset shows the experimental line profile across one of the Cu_2O crystals. (c and d) Nano-IR amplitude $s(\omega)$ images of Cu_2O at two different IR frequencies.

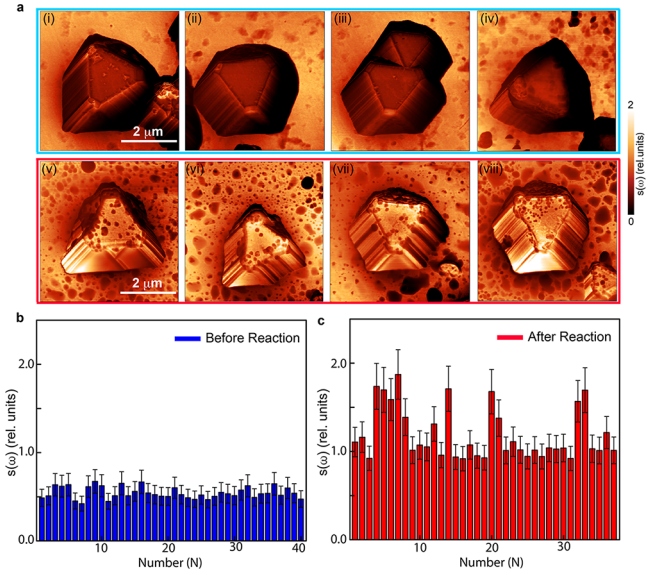

Figure 2. Nano-IR imaging of Cu_2O microcrystals before and after electrochemical reactions. (a) Representative images of nano-IR amplitude $s(\omega)$ collected for Cu_2O microcrystals. Panels (i) to (iv) show nanoimages of Cu_2O before reaction, whereas panels (v) to (viii) show the results after chemical reaction in $KHCO_3$ solution (see Supporting Information, p S1). In these experiments the incident IR laser frequency was fixed at $\omega = 905$ cm^{-1}. (b, c) Statistics of the $s(\omega)$ signal for Cu_2O microcrystals in their pristine state (panel b) and after chemical reactions (panel c). In (b) and (c), each data point represents one image.

of the response function of the catalyst microparticles such as the complex dielectric function $\varepsilon(\omega)$, as will be detailed below.

We begin with nano-IR characterization of pristine Cu_2O microcrystals at ambient conditions. We found that as-grown Cu_2O microcrystals predominantly exhibit triangular platelet geometry, with well-defined facets. Figure 1b show atomic force microscope (AFM) topography of representative pristine Cu_2O single crystals on top of a $PPC/SiO_2/Si$ substrate (Methods). In Figure 1c,d, we show representative nano-IR imaging data collected at different IR frequencies. Here we plot raster-scanned images of the normalized back scattering amplitude signal $s(\omega)$ at two selected IR frequencies, ω = 928 and $\omega = 1030$ cm^{-1}, respectively. From these images, we found that (i) Cu_2O polyhedral microcrystals exhibited clear near-field contrast compared with the substrate; (ii) little variations of Cu_2O near-field responses existed between 928 and 1030 cm^{-1}, suggesting a featureless dielectric function of Cu_2O crystals within this frequency range.

We now present our key nanoimaging results for Cu_2O microcrystals before and after electrochemical reduction of CO_2 (Figure 2). In Figure 2a(i–iv), we show the raster-scanned results for pristine Cu_2O microcrystals on a conductive glassy carbon substrate. The same Cu_2O film on a glassy carbon substrate was used as an electrode for electrochemical reduction of CO_2. The nanoimaging results are shown in Figure 2a(v–viii). By comparing the results acquired for the pristine specimens and samples after electrochemical CO_2 reduction, we have identified a number of systematic trends: (i) after electrochemical reduction of CO_2 the reacted Cu_2O microcrystals largely maintain their triangular form as in the pristine state, other than the appearance of chemical residues randomly distributed on the sample surface; (ii) one of the most prominent differences is that the near-IR signal due to the reacted Cu_2O crystals is enhanced compared to that of the pristine counterparts. For quantitative analysis, we have examined more than 80 different Cu_2O microcrystals before and after catalytic reactions, and the corresponding statistics are shown in Figure 2b,c. In Figure 2b, we present the normalized near-field amplitude $s(\omega)$ for the pristine Cu_2O microcrystals using the common nano-IR signal of the glassy carbon substrate as a reference; the averaged $s(\omega)$ for the totality of samples we imaged is close to 0.5. Figure 2c shows the results after catalysis reactions; in these latter data the area-average signal $s(\omega)$ has increased above 1. This clear difference between pristine and CO_2-exposed Cu_2O microcrystals attests to the profound chemical modifications that are captured via our unique nano-optical probe.

To understand radical changes in nanoimaging results for pristine and reacted microparticles after electrochemical reduction of CO_2, we performed nano-FTIR spectroscopic studies, which allows us to evaluate the local permittivity and resonances over a broad frequency range at the nanoscale. In Figure 3, we show nanospectroscopy results for Cu_2O microcrystals before and after chemical reactions. To acquire these images, we have intentionally chosen the frequency region that contains the phonon resonance of Cu_2O. In Figure 3a,b we present the raw data (solid red curve) of the normalized near-field amplitude $s(\omega)$ and phase $\phi(\omega)$ for pristine Cu_2O samples. A pronounced resonance centered at ~640 cm^{-1} is evident in these data (solid red curves in Figure 3a,b). To verify the origin of this resonance, we analyzed the near-field signal within the framework of the lighting rod model. In this model, the near-field interaction between AFM probe and Cu_2O sample is evaluated numerically and incorporates the AFM tip radius a and its geometry, tapping amplitude, incident frequency ω, and the dielectric function $\varepsilon(\omega)$ of the host material.[26,27] In these calculations, the experimentally obtained far-field dielectric function $\varepsilon(\omega)$ =

https://dx.doi.org/10.1021/acsphotonics.9b01704
ACS Photonics 2020, 7, 576–580

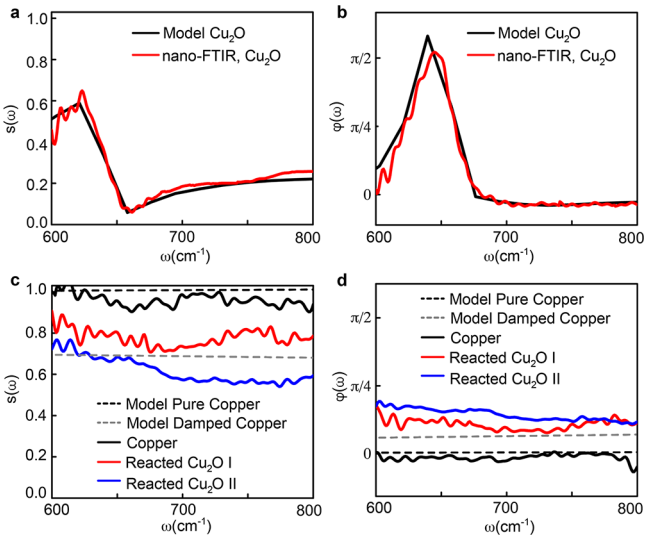

Figure 3. Fourier Transform infrared nanospectroscopy (nano-FTIR) of Cu_2O microcrystals before and after electrochemical reactions. (a, b) Normalized near-field amplitude $s(\omega)$ and phase $\varphi(\omega)$ for a Cu_2O microcrystal in its pristine state. Red: data, black: modeling results obtained as explained in the main text. (c, d) Nano-FTIR spectra for Cu_2O after chemical reaction taken from the areas examined by the AFM topography. The red and blue traces are the normalized near-field spectra obtained for Cu_2O microcrystals, whereas the black curves correspond to near-field signal from pure copper foil. The dashed traces are the modeling results for pure copper and heavily disordered copper, respectively.

$\varepsilon_1(\omega) + i\varepsilon_2(\omega)$ of Cu_2O was used as input for modeling the near-field signal.[28] The calculated near-field spectra exhibited excellent agreement with the experimental nano-FTIR data (Figure 3a,b). This agreement attests that the strong phonon resonance of Cu_2O gives rise to the observed features.

In contrast, nearly featureless spectra are obtained for the reaction-modified Cu_2O microcrystals. In Figure 3c,d, we show two sets of spectra obtained for different Cu_2O samples. Other than a slight variation of the near-field amplitude, the two data sets share identical features across the examined frequencies. We also performed nano-FTIR studies on pure copper foil, which serves as the reference sample. To model these latter data, we used the pure copper dielectric function $\varepsilon(\omega)$ ($\varepsilon_1(\omega) \ll 0$; $\varepsilon_2(\omega) \gg 0$) as the input parameter.[30] As expected, the calculated pure copper near-field signal matches well with the experimental near-field data from the pure copper foil (Figure 3c,d). Specifically, the near-field amplitude $s(\omega)$ of pure copper approaches unity, while the near-field phase $\phi(\omega)$ remains negligible. Our modeling shows that in order to capture the experimental results for the chemically reacted Cu_2O, it is not sufficient to only increase the copper foil damping rate. In fact, a reasonably good fit requires the input parameter $\varepsilon_1(\omega)$ to become positive in the frequency range of our measurements (Figure 3c,d). We therefore conclude that the chemically reacted Cu_2O does not necessarily transform into the pure copper, as commonly believed.[31,32] It is likely that the chemically exposed Cu_2O catalyst reveals modified electronic properties, including a strongly reduced energy gap that needs to be explored in follow-up investigations.[33−35] In short, we have examined dozens of samples with different sizes, and our results are consistent with each other. This difference is also confirmed by our catalytic results displayed in the Supporting Information (Figure S3). When Cu foil was employed as the catalysts for the electrochemical reduction of CO_2, the hydrogen evolution reaction dominated the process where hydrogen has the highest faradic efficiency. On the other hand, when Cu_2O polyhedral microcrystals acted as the catalysts, the faradic efficiency of ethylene and ethanol increased 10 and 4 times over those of Cu foil, respectively. Another interesting observation is the enhanced near-field contrast at sample edges. After chemical reactions, it is found that the corresponding near-field signal at the edge/corner is higher than in the interior surface area of microcrystals (Figure 2). This observation suggests that the chemical reactivity at the crystal edges is higher than the sample surface, which agrees with the interpretation of data in previous reports.[36−38]

Our experimental results, together with parameter-free theoretical modeling, provided new insights into electrochemical reactions and catalyst reduction at the nanoscale. These observations illustrate the merits of nano-IR imaging and nano-IR spectroscopy for direct monitoring of complex chemical processes on the surface of microcrystals. Looking to the future, we envision real-time and real-space monitoring of catalytic reactions and energy conversions[39] at the nanoscale. This can be readily accomplished by incorporating two-dimensional membranes and further plasmonic enhancement[40] as nano-optical compatible lids of reacting cells in vivo.[41]

METHODS

Sample Synthesis. The Cu_2O nanoparticles were fabricated via the aqueous sol−gel method (see Supporting Information). The solution was prepared by dissolving the calculated amount of $CuCl_2$ (170 mg) and PVP40 (3.3 g) in 80 mL of deionized water. The compound was separated out by filtration and washed with deionized water and ethanol multiple times to remove unreacted chemicals.

Nano-IR Imaging. The infrared nanoimaging experiments were performed using s-SNOM equipped with continuous-wave mid-IR quantum cascade lasers (daylightsolutions.com). The s-SNOM is based on AFM with a curvature radius ~25 nm operating in the tapping mode with a tapping frequency around 270 kHz. A pseudoheterodyne interferometric detection module was implemented to extract both the scattering amplitude s and the phase of the near-field signal. In the current work, we discuss the amplitude of the signal. In order to subtract the background signal, we demodulated the near-field signal at the third harmonics of the tapping frequency. All the infrared nanoimaging experiments were performed in ambient conditions. We used quantum cascade lasers with tunable frequency and a broad-band difference frequency generation laser system.

ASSOCIATED CONTENT

Supporting Information

The Supporting Information is available free of charge at https://pubs.acs.org/doi/10.1021/acsphotonics.9b01704.

Materials and methods (PDF)

AUTHOR INFORMATION

Corresponding Authors

G. Chen − *Honda Research Institute USA, Inc., San Jose, California 95134, United States;* orcid.org/0000-0003-3798-320X; Email: gchen@honda-ri.com

https://dx.doi.org/10.1021/acsphotonics.9b01704
ACS Photonics 2020, 7, 576−580

D. N. Basov − *Department of Physics, Columbia University, New York, New York 10027, United States*; Email: db3056@columbia.edu

Authors

G. X. Ni − *Department of Physics, Columbia University, New York, New York 10027, United States*; orcid.org/0000-0002-7216-1829

S. Chen − *Honda Research Institute USA, Inc., San Jose, California 95134, United States*

S. S. Sunku − *Department of Physics and Department of Applied Physics and Applied Mathematics, Columbia University, New York, New York 10027, United States*; orcid.org/0000-0002-7037-8717

A. Sternbach − *Department of Physics, Columbia University, New York, New York 10027, United States*

A. S. McLeod − *Department of Physics, Columbia University, New York, New York 10027, United States*

L. Xiong − *Department of Physics, Columbia University, New York, New York 10027, United States*

M. M. Fogler − *Department of Physics, University of California, San Diego, La Jolla, California 92093, United States*

Complete contact information is available at: https://pubs.acs.org/10.1021/acsphotonics.9b01704

Author Contributions

All authors were involved in designing the research, performing the research, and writing the paper.

Notes

The authors declare no competing financial interest.

■ ACKNOWLEDGMENTS

The development of novel nanoimaging capabilities is supported as part of Programmable Quantum Materials, an Energy Frontier Research Center funded by the U.S. Department of Energy (DOE), Office of Science, Basic Energy Sciences (BES), under award DE-SC0019443. The initial phase of the experimental work was supported by the Honda Research Institute USA, Inc. The authors acknowledge help from Daniel Esposito and Anna Elisabeth Dorfi.

■ REFERENCES

(1) Angamuthu, R.; Byers, P.; Lutz, M.; Spek, A. L.; Bouwman, E. Electrocatalytic CO_2 conversiontooxalateby a coppercomplex. *Science* **2010**, *327*, 313−315.

(2) Medina-Ramos, J.; DiMeglio, J. L.; Rosenthal, J. Efficientreductionof CO_2 to CO with high currentdensityusing in situ or ex situ prepared Bi-basedmaterials. *J. Am. Chem. Soc.* **2014**, *136*, 8361−8367.

(3) Richardson, R. D.; Holland, E. J.; Carpenter, B. K. A reneableamineforphotochemicalreductionof CO_2. *Nat. Chem.* **2011**, *3*, 301−303.

(4) Rosen, B. A.; et al. Ionic liquid-mediatedselectiveconversionof CO_2 to CO at lowoverpotentials. *Science* **2011**, *334*, 643−644.

(5) Zhang, L.; Zhu, D.; Nathanson, G. M.; Hamers, R. J. Selectivephotoelectrochemicalreductionofaqueous CO_2 to CO by-solvatedelectrons. *Angew. Chem., Int. Ed.* **2014**, *53*, 9746−9750.

(6) Gao, D.; et al. Size-dependentelectrocatalyticreductionof CO_2 overPdnanoparticles. *J. Am. Chem. Soc.* **2015**, *137*, 4288−4291.

(7) Mistry, H.; et al. Exceptionalsize-dependentactivityenhancement in theelectroreductionof CO_2 over Au nanoparticles. *J. Am. Chem. Soc.* **2014**, *136*, 16473−16476.

(8) Reske, R.; Mistry, H.; Behafarid, F.; Roldan Cuenya, B.; Strasser, P. Particlesizeeffects in thecatalyticelectroreductionof CO_2 on Cunanoparticles. *J. Am. Chem. Soc.* **2014**, *136*, 6978−6986.

(9) Zhu, W.; et al. Monodisperse Au nanoparticlesforselectiveelectrocatalyticreductionof CO_2 to CO. *J. Am. Chem. Soc.* **2013**, *135*, 16833−16836.

(10) Salehi-Khojin, A.; et al. Nanoparticles silver catalysts that show enhanced activity for carbon dioxide electrolysis. *J. Phys. Chem. C* **2013**, *117*, 1627−1632.

(11) LaGrow, A.; et al. VisualizingtheCu/Cu_2O interfacetransition in nanoparticleswith environmental scanningtransmissionelectronmicroscopy. *J. Am. Chem. Soc.* **2017**, *139*, 179−185.

(12) Wang, Y.; et al. Dynamic deformabilityof individual PbSenanocrystalsduringsuperlatticephasetransitions. *Science Advances* **2019**, *5*, No. eaaw5623.

(13) Zhu, C.; et al. In-situ liquid celltransmissionelectronmicroscopyinvestigation on orientedattachmentofgoldnanoparticles. *Nat. Commun.* **2018**, *9*, 421.

(14) Wu, C. Y.; et al. High-spatial-resolution mappingofcatalytic-reactions on singleparticles. *Nature* **2017**, *541*, 511.

(15) Johnson, C. M.; Böhmler, M. Nano-FTIR microscopyandspectroscopystudiesofatmosphericcorrosionwith a spatialresolutionof 20 nm. *Corros. Sci.* **2016**, *108*, 60−65.

(16) Ross, M. B.; et al. Designing Materials forElectrochemical Carbon Dioxide Recycling. *Nature Catalysis* **2019**, *2*, 648−658.

(17) Birdja, Y. Y.; et al. Advancesandchallenges in understandingtheelectrocatalyticconversionofcarbondioxidetofuels. *Nature Energy* **2019**, *4*, 732−745.

(18) Kas, R.; et al. Electrochemical CO_2 reduction on Cu_2O-derived coppernanoparticles: controllingthecatalyticselectivityofhydrocarbons. *Phys. Chem. Chem. Phys.* **2014**, *16*, 12194−12201.

(19) Jiang, K.; et al. Metal ion cycling of Cu foil for selective C−C coupling in electrochemical CO_2 reduction. *Nature Catalysis* **2018**, *1*, 111−119.

(20) Luna, P. D.; et al. Catalyst electro-redeposition controls morphology and oxidation state for selective carbon dioxide reduction. *Nat. Catal.* **2018**, *1*, 103−110.

(21) Wan, L.; et al. Cu_2O nanocubeswithmixedoxidation-statefacetsfor (photo)catalytichydrogenationofcarbondioxide. *Nature Catalysis* **2019**, *2*, 889.

(22) Post, K. W.; et al. Coexisting first- and second-order electronic phasetransitions in a correlatedoxide. *Nat. Phys.* **2018**, *14*, 1056.

(23) Ni, G. X.; et al. Plasmons in graphenemoirésuperlattices. *Nat. Mater.* **2015**, *14*, 1217−1222.

(24) Denyer, M.; Micheletto, R.; Nakajima, K.; Hara, M.; Okazaki, S. Biological imagingwith a near-fieldopticalsetup. *J. Nanosci. Nanotechnol.* **2003**, *3*, 496−502.

(25) Srinivasarao, M. Nano-optics in thebiologicalworld: Beetles, Butterflies, Birds, and Moths. *Chem. Rev.* **1999**, *99*, 1935−1962.

(26) Yang, H. U.; Hebestreit, E.; Josberger, E. E.; Raschke, M. B. *Rev. Sci. Instrum.* **2013**, *84*, 023701.

(27) Ni, G. X.; et al. Ultrafast optical switching of infrared plasmonpolaritons in high-mobility graphene. *Nat. Photonics* **2016**, *10*, 244−247.

(28) Ni, G. X.; et al. Fundamental limits to graphene plasmonics. *Nature* **2018**, *557*, 530−533.

(29) Sunku, S. S.; et al. Photonic crystals for nano-light in moire graphene superlattices. *Science* **2018**, *362*, 1153.

(30) Querry, M. R. Optical constants. *Contractor Report CRDC-CR-85034*, Defense Technical Information Center, 1985.

(31) Kim, J. Y.; et al. Reduction of CuO and Cu_2O with H_2: embedding and kinetic effects in the formation of sub oxides. *J. Am. Chem. Soc.* **2003**, *125*, 10684.

(32) Nakayama, S.; Kaji, T.; Shibata, M.; Notoya, T.; Osakai, T. Whichiseasiertoreduce, Cu_2O orCuO? *J. Electrochem. Soc.* **2007**, *154*, C1.

(33) Lee, S.; Kim, D.; Lee, J. ElectrocatalyticProductionof C3-C4 Compounds by Conversionof CO2 on a Chloride-Induced Bi-Phasic Cu_2O-Cu Catalyst. *Angew. Chem., Int. Ed.* **2015**, *54*, 14701−14705.

(34) Mistry, H.; et al. HighlySelective Plasma-ActivatedCopperCatalystsfor Carbon Dioxide Reduction to Ethylene. *Nat. Commun.* **2016**, *7*, 1−8.

(35) Fields, M.; Hong, X.; Norskov, J. K.; Chan, K. Roleofsubsurfaceoxygen on Cusurfacesfor CO_2 electrochemicalreduction. *J. Phys. Chem. C* **2018**, *122*, 16209−15.
(36) Huang, L.; et al. Shape regulationof high-index facetnanoparticlesbydealloying. *Science* **2019**, *365*, 1159−1163.
(37) Quan, Z.; Wang, Y.; Fang, J. High-Index Faceted Noble Metal Nanocrystals. *Acc. Chem. Res.* **2013**, *46*, 191−202.
(38) Ni, B.; Wang, X. Face theEdges: Catalytic Active Sites of Nanomaterials. *Advanced Science* **2015**, *2*, 1500085.
(39) Li, Y.; Somorjai, G. A. Nanoscale advances in catalysis and energy applications. *Nano Lett.* **2010**, *10*, 2289.
(40) Linh, V. T. N.; et al. Compact integration of TiO_2 nanoparticles into the cross-points of 3D vertically stacked Ag nanowires for plasmon-enhanced photocatalysis. *Nanomaterials* **2019**, *9*, 468.
(41) Khatib, O.; et al. Graphene-based platform for infrared near-field nanospectroscopy of water and biological materials in an aqueous environment. *ACS Nano* **2015**, *98*, 7968−7975.

https://dx.doi.org/10.1021/acsphotonics.9b01704
ACS Photonics 2020, 7, 576−580

Supplementary Information

Nanoscale infrared spectroscopy and imaging of catalytic reactions in Cu_2O crystals

G. X. Ni[1*], S. Chen[2], S. S. Sunku[1,4], A. Sternbach[1], A. S. McLeod[1], L. Xiong[1], M. M. Fogler[3], G. Chen[2†], D. N. Basov[1†]

[1]Department of Physics, Columbia University, New York, USA.
[2]Honda Research Institute USA, Inc., 70 Rio Robles, San Jose, California 95134, USA.
[3]Department of Physics, University of California, San Diego, La Jolla, California 92093, USA.
[4]Department of Applied Physics and Applied Mathematics, Columbia University, New York, USA.
[*]Current address: Department of Physics, Florida State University, Tallahassee, Florida 32310, United States; National High Magnetic Field Laboratory, Florida State University, Tallahassee, Florida, 32310, United States.
[†]Corresponding authors. Email: gchen@honda-ri.com; db3056@columbia.edu.

1. Synthesis of Cu_2O polyhedral microcrystals

To synthesis Cu_2O polyhedral microcrystals, 170 mg of copper (II) chloride dihydrate ($CuCl_2 \cdot 2H_2O$) was dissolved in 80 ml de-ionized water, followed by an addition of 3.3 g PVP40 and stirring thoroughly until PVP40 had been dissolved completely. 10 ml of 2 M NaOH aqueous solution was added dropwise into the above solution. After 30 min of stirring, 10 ml of 0.6 M Vitamin C was applied dropwise into the mixture solution and the reaction was continued for 3 h at 90 °C. During this procedure, the color of the solution changed into light blue, dark blue and eventually turbid red. All of these processes were carried out under constant stirring and at a fixed flask temperature of 90 °C. The resulting precipitate was collected by centrifugation and washed with de-ionized water and ethanol multiple times to remove unreacted chemicals. Finally, it was dried at 70 ^{o}C in a vacuum oven overnight.

2. Characterization of Cu_2O polyhedral microcrystals

The surface morphologies of Cu_2O polyhedral microcrystals were investigated by scanning electron microscope (SEM) from FEI (QUANTA FEG 650) (SFig. 1). A Bruker D8 Advance X-ray diffractometer with Cu Kα radiation operated at a tube voltage of 30 kV and a current of 40 mA was used to obtain X-ray diffraction (XRD) patterns. Gas chromatograph (GC 17A, SHIMADZU) was employed to analyze the concentration of the gas products. The separated gas products were analyzed by a thermal conductivity detector (for H_2) and a flame ionization detector (for CO, CH_4, and C_2H_4). Liquid products (formic acid, and ethanol) were analyzed by high performance liquid chromatograph (HPLC) with Dionex UltiMate 3000 (UHPLC+, Thermo Scientific).

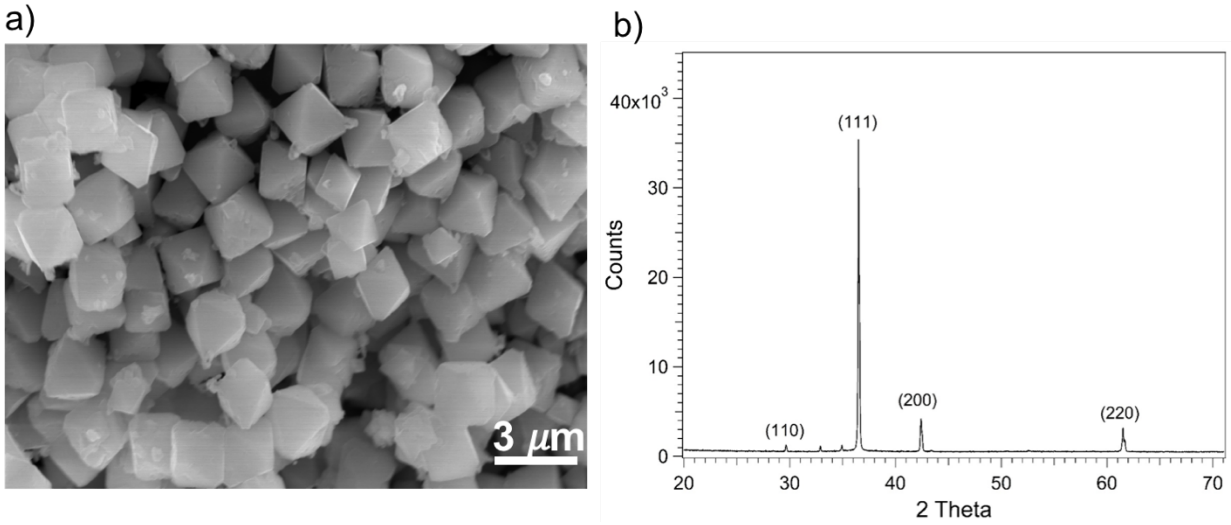

Figure S1 a) Scanning electron microscope image and b) XRD of Cu_2O polyhedral microcrystals.

3. Electrochemical measurements

Electrochemical CO_2 reduction experiments were conducted using a potentiostat (VersaSTAT MC) in a two compartment electrochemical cell separated by an anion-exchange membrane (Selemion AMV).[1] A platinum plate counter electrode and a leak-free Ag/AgCl reference electrode (Innovative Instruments, diameter: 1.0 mm) were used in a three electrode configuration. Working electrodes were prepared by drop-casting 500 μg of Cu_2O polyhedral microcrystals (Cu_2O

polyhedral microcrystals were dispersed in DI water) onto a glassy carbon electrode (Alfa Aesar: diameter of 1.0 cm) and drying under argon at room temperature. The working electrode and the counter electrode compartment hold 2.0 mL of electrolyte each. The working compartment was sealed in order to measurement the gas products. All potentials in this work are converted to the RHE scale by the following formula: E (vs RHE) = E(vs Ag/AgCl) + 0.205 V + 0.0591 × pH. A 0.1 M $KHCO_3$ electrolyte was prepared from K_2CO_3 saturated with CO_2 (pH 7.5).

During electrochemical reactions, CO_2 flowed through the working compartment at a rate of 5 sccm. Effluent gas from the cell went through the sampling loop of the GC to analyze the concentration of gas products. Quantification of the gas products was performed with the conversion factor derived from standard calibration gases. Liquid products were analyzed afterward by HPLC. The concentrations were calculated based on the calibration curves which we developed for each individual component. Faradaic efficiencies were calculated from the amount of charge passed to produce each product, divided by the total charge passed at a specific time or during the overall run (SFig. 2).

SFigure 2 shows the current vs. time profile of a representative electrolysis experiment at -1.05 V vs. RHE. The average current density of Cu_2O polyhedral microcatalysts remain at 2.52 mA/cm^2 across the 2.5 hour-long testing. SFigure 3 summarizes the results of electrochemical studies of Cu foil and Cu_2O polyhedral microcatalysts at -1.05 V vs. RHE. Compared to Cu foil, Cu_2O polyhedral microcatalysts have shifted the reaction more to CO_2 reduction instead of H_2 generation. In addition, the faradic efficiency (FE) of C_2H_4 can reach 19.8% when Cu_2O is employed as the catalysts. Cu_2O catalyst is also more selective to formic acid and ethanol productions, and their FE can reach 7.5% and 8.6%, respectively.

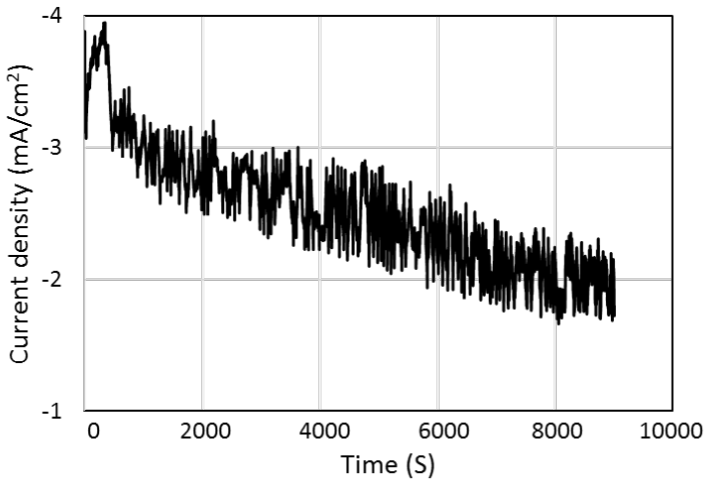

Figure S2 Chronoamperometry curve of CO_2 reduction reaction on Cu_2O polyhedral microcatalysts in 0.1 M $KHCO_3$ electrolyte at a potential of -1.05 V vs. RHE.

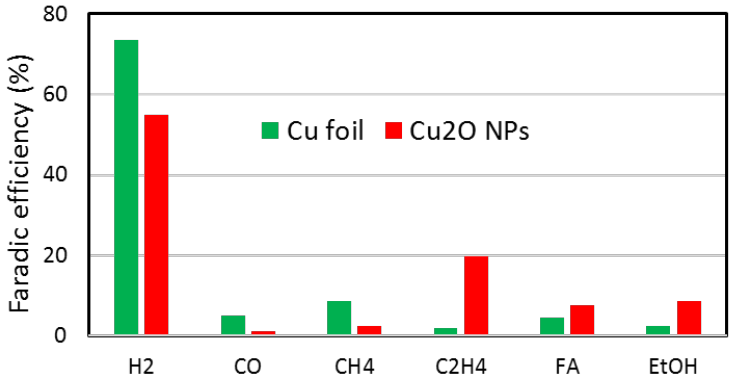

Figure S3 Electrocatalytic activity of Cu foil and Cu_2O polyhedral microcatalysts for electrochemical reduction of CO_2 at -1.05 V vs RHE.

4. Nano-IR measurements

One interesting effect that we observed is that the edges are brighter than the center of the particles after electrochemical reaction (Fig. 2 of the main text). To better visualize the edge-interior difference, we examined the near-field signal at edges of the samples and compared these data with the images acquired in the interior of the crystal, as shown in Figure S4. Clearly, the signal at the edge is much higher than the interior of the crystals. By analyzing massive amount of specimens with different illuminated edges, we rule out topographic edge/artifacts as the primary source of this contrast.

Moreover, we obtained nano-IR spectra close to the edges (Figure S5). These data clearly show that close the sample edge, the near-field signal are indistinguishable from that of pure copper (Figure S5). This latter finding indicates that edges are indeed more reactive and can be readily transformed into metallic copper via electrochemical reactions. Contrary to these observations, the interior of the crystal remains insulating with a finite energy gap as discussed in the main text. In short, our observations clearly reveal the spatially-resolved nano-catalysis at the nanoscales.

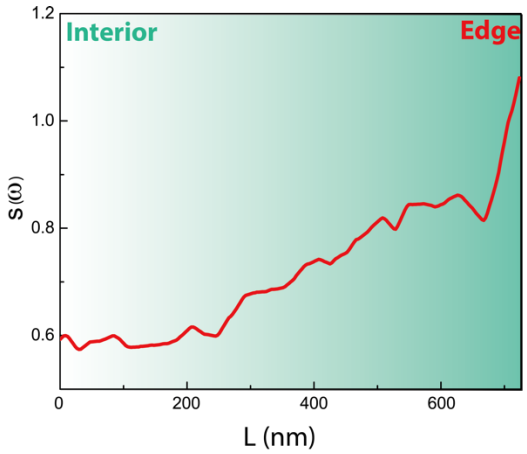

Figure S4. Line-profile of the extracted near-field signal of Cu_2O microcrystals after electrochemical reactions. one can clearly visualize the spatial change along the particle surfaces from edge to the interior of the crystal.

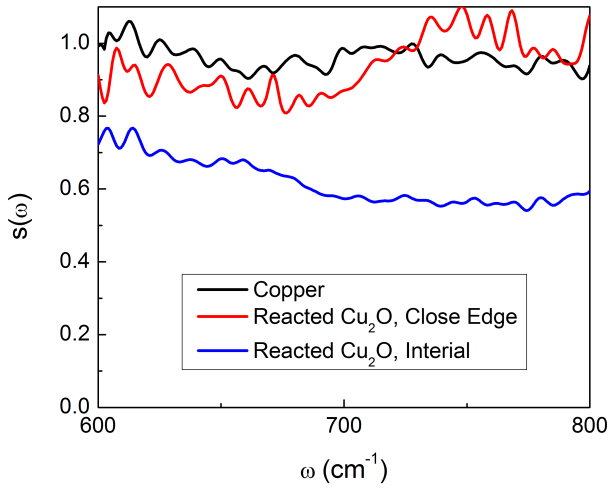

Figure S5. Fourier Transform infrared nano-spectroscopy (nano-FTIR) of Cu_2O microcrystals after electrochemical reactions. The black trace is the normalized near-field spectrum obtained for pure copper. Red and blue traces are the normalized near-field spectra obtained at the edge and the center of the Cu_2O microcrystals, respectively. In our studies, we had examined the AFM topography images carefully to identify the flat & clean

areas for subsequent nano-spectoscopy investigations.

References:

1. K. P. Kuhl, E. R. Cave, D. N. Abram, T. F. Jaramillo, “New insight into the electrochemical reduction of carbon dioxide on metallic copper surface”, *Energy Environment Science*, 5, 7050-7059, 2012.